

Dynamical Mean-Field Theory of Complex Systems on Sparse Directed Networks

Fernando L. Metz¹*Physics Institute, Federal University of Rio Grande do Sul, 91501-970 Porto Alegre, Brazil*

(Received 12 June 2024; revised 4 October 2024; accepted 20 December 2024; published 24 January 2025)

Although real-world complex systems typically interact through sparse and heterogeneous networks, analytic solutions of their dynamics are limited to models with all-to-all interactions. Here, we solve the dynamics of a broad range of nonlinear models of complex systems on sparse directed networks with a random structure. By generalizing dynamical mean-field theory to sparse systems, we derive an exact equation for the path probability describing the effective dynamics of a single degree of freedom. Our general solution applies to key models in the study of neural networks, ecosystems, epidemic spreading, and synchronization. Using the population dynamics algorithm, we solve the path-probability equation to determine the phase diagram of a seminal neural network model in the sparse regime, showing that this model undergoes a transition from a fixed-point phase to chaos as a function of the network topology.

DOI: [10.1103/PhysRevLett.134.037401](https://doi.org/10.1103/PhysRevLett.134.037401)

Introduction—Complex dynamical systems are modeled by N degrees of freedom $x_i(t)$ ($i = 1, \dots, N$) that evolve in time according to the differential equation

$$\dot{x}_i(t) = -f(x_i) + \sum_{j=1}^N A_{ij}g(x_i, x_j), \quad (1)$$

where $\{A_{ij}\}_{i,j=1,\dots,N}$ defines the interaction network. The function $f(x)$ governs the dynamics in the absence of interactions, and the kernel $g(x, x')$ shapes the pairwise couplings. Equation (1) models the nonequilibrium dynamics of neural networks [1–5] and ecosystems [6–8], epidemic spreading [9–12], synchronization phenomena [13–15], opinion dynamics [16,17], and multivariate Ornstein-Uhlenbeck processes [18–20]. Table I specifies $f(x)$ and $g(x, x')$ for paradigmatic models of complex behavior.

The foremost problem in the study of complex systems is how to reduce the dynamics of many interacting elements to the dynamics of a few variables [23]. Dynamical mean-field theory (DMFT) [24–26] is a powerful method to tackle this problem in the limit $N \rightarrow \infty$, yielding a solution in terms of the path probability for the effective dynamics of a single degree of freedom. The application of DMFT to models described by Eq. (1) has been attracting an enormous interest [2–5,7,8,15,19,20,27–34], especially in the context of neural networks and ecosystems. Phase diagrams of these models reveal a rich phenomenology, including different types of phase transitions [5,7,30], chaotic behavior [1,3], and coexistence of multiple attractors [7,8,35]. Despite this substantial theoretical progress, DMFT is currently limited to dense networks, where each dynamical variable

is essentially coupled to *all* others by means of Gaussian interaction strengths. However, the interactions in real-world complex systems are known to be *sparse* and *heterogeneous* [36,37]. Sparseness indicates that each element of the system interacts on average with a finite number of others, while heterogeneity refers to fluctuations in the local topology of the interaction network. How to integrate these more realistic features in the formalism of DMFT for systems modeled by Eq. (1) remains an unresolved challenge, and even basic questions, such as deriving the phase diagram of sparse complex systems, are still out of reach.

On the other hand, the dynamics of complex systems on sparse networks has been extensively studied in the case of Ising spins [38–50]. In this context, both the cavity method [39] and DMFT [38,40] provide an analytic solution in terms of the path probability for the effective dynamics of a single dynamical variable. However, the presence of bidirected edges induces a temporal feedback, which, in the particular case of sparse systems, leads

TABLE I. Explicit form of $f(x)$ and $g(x, x')$ in complex systems modeled by Eq. (1). Equation (1) for the SIS model is derived through the quenched mean-field approximation [12,21,22].

Model	$f(x)$	$g(x, x')$
Ornstein-Uhlenbeck process [18]	x	x'
SIS model of epidemic spreading [9]	x	$(1 - x)x'$
Lotka-Volterra (LV) model [7,8]	$x(x - 1)$	xx'
Neural network (NN) model [1,4]	x	$\tanh(x')$
Kuramoto model [14]	0	$\sin(x' - x)$

to an exponential growth of the path-probability dimension [38,40,49], rendering numerical computations unfeasible. Approximation schemes, such as the one-time approximation [39], make these computations possible [42,43,48]. When the interactions are directed or unidirectional, there is no temporal feedback and the path-probability equation can be efficiently solved [38,39,51].

Inspired by these results for Ising spins, in this Letter we solve the dynamics of models governed by Eq. (1) on sparse directed networks with an heterogeneous topology. The solution represents a foundational step in the study of complex systems, as it ultimately incorporates the sparse and heterogeneous structure of complex networks into the formalism of DMFT. Directed networks are interesting because they model the nonreciprocal interactions in real-world complex systems [52], including the human cortex [53], food webs [37,54,55], gene regulatory networks [56,57], online social networks [58,59], and the World Wide Web [60]. The formalism presented here thus opens the possibility to analytically investigate how realistic interactions impact the dynamics of complex systems.

By generalizing DMFT to sparse systems, we obtain an exact equation for the path probability describing the effective dynamics of a single variable for $N \rightarrow \infty$, and we solve this equation for different models in Table I by using the population dynamics algorithm [61–66]. The excellent agreement between our theoretical results and numerical simulations of finite systems confirms that our solution applies to various nonlinear models interacting through different network topologies, including networks with power-law degree distributions [36].

As an application, we determine the phase diagram of the neural network model by Sompolinsky *et al.* [1] in the sparse regime. We show that the phase diagram displays trivial and nontrivial fixed-point phases, a chaotic phase with zero mean activity, and a chaotic phase with nonzero mean activity [30]. By calculating certain macroscopic observables, we determine the transition lines as functions of the mean degree and the variance of the coupling strengths, showing their consistency with the universal critical lines derived from random matrix theory [67–69]. In particular, we provide numerical evidence that the transition between the chaotic phases coincides with the vanishing of the gap between the leading and the subleading eigenvalue of the interaction matrix.

Sparse directed networks—Let $A_{ij} = C_{ij}J_{ij}$ be the elements of the $N \times N$ interaction matrix \mathbf{A} . The binary variables $C_{ij} \in \{0, 1\}$ determine the network topology, while $J_{ij} \in \mathbb{R}$ controls the interaction strengths. If $C_{ij} = 1$, there is a directed edge $j \rightarrow i$ pointing from node j to i , while $C_{ij} = 0$ otherwise. The indegree $K_i = \sum_{j=1}^N C_{ij}$ and the outdegree $L_i = \sum_{j=1}^N C_{ji}$ count the number of links entering and leaving node i [36], respectively. The random variables $\{C_{ij}\}_{i \neq j}$ follow the distribution

$$\mathbb{P}(\{C_{ij}\}) = \frac{1}{\mathcal{N}} \prod_{i \neq j=1}^N \left[\frac{c}{N} \delta_{C_{ij},1} + \left(1 - \frac{c}{N}\right) \delta_{C_{ij},0} \right] \times \prod_{i=1}^N \delta_{K_i, \sum_{j=1}^N C_{ij}} \delta_{L_i, \sum_{j=1}^N C_{ji}}, \quad (2)$$

where \mathcal{N} is the normalization constant and $C_{ii} = 0$. The degrees $\{K_i, L_i\}_{i=1, \dots, N}$ are independent and identically distributed random variables drawn from $p_{k,\ell} = p_{\text{in},k} p_{\text{out},\ell}$, where $p_{\text{in},k}$ and $p_{\text{out},\ell}$ are the indegree and the outdegree distribution [36,64], respectively. The parameter c is the average degree

$$c = \sum_{k=0}^{\infty} k p_{\text{in},k} = \sum_{\ell=0}^{\infty} \ell p_{\text{out},\ell}. \quad (3)$$

Equation (2) defines a network ensemble where directed links are randomly placed between pairs of nodes with probability c/N , subject to the prescribed degree sequences generated from $p_{k,\ell}$. In the limit $N \rightarrow \infty$, network samples generated from Eq. (2) are similar to those produced by the configuration model [70,71]. The coupling strengths $\{J_{ij}\}_{i,j=1, \dots, N}$ are independent and identically distributed random variables drawn from a distribution p_J with mean μ_J and variance σ_J^2 . The distributions $p_{k,\ell}$ and p_J fully specify the network ensemble, allowing for a systematic investigation of how network heterogeneities impact the dynamics of complex systems.

Solution through DMFT—We solve the coupled dynamics of Eq. (1) on directed networks by using dynamical mean-field theory (DMFT) [24–26]. We consider the sparse regime, where the mean degree c is *finite*, independent of N . DMFT is based on the generating functional

$$\mathcal{Z}[\boldsymbol{\psi}] = \int \left(\prod_{i=1}^N D x_i \right) \mathcal{P}[\mathbf{x}] e^{i \int dt \sum_{i=1}^N x_i(t) \psi_i(t)} \quad (4)$$

of the probability density $\mathcal{P}[\mathbf{x}]$ of observing a dynamical path of states $\mathbf{x}(t) = [x_1(t), \dots, x_N(t)]$ in a fixed time interval. The correlation functions of $\{x_i(t)\}_{i=1, \dots, N}$ follow from the derivatives of $\mathcal{Z}[\boldsymbol{\psi}]$ with respect to the external sources $\boldsymbol{\psi}(t) = [\psi_1(t), \dots, \psi_N(t)]$. The n th moment of the local variable $x_i(t)$,

$$\langle x_i^n(t) \rangle = \int \left(\prod_{i=1}^N D x_i \right) x_i^n(t) \mathcal{P}[\mathbf{x}] = (-i)^n \frac{\delta^n \mathcal{Z}[\boldsymbol{\psi}]}{\delta \psi_i^n(t)} \Big|_{\boldsymbol{\psi}=0}, \quad (5)$$

yields the time evolution of the macroscopic quantities

$$m(t) = \lim_{N \rightarrow \infty} \frac{1}{N} \sum_{i=1}^N \langle x_i(t) \rangle, \quad q(t) = \lim_{N \rightarrow \infty} \frac{1}{N} \sum_{i=1}^N \langle x_i^2(t) \rangle. \quad (6)$$

Clearly, $\mathcal{Z}[\psi]$ fulfills $\mathcal{Z}[0] = 1$.

In [72], we calculate the average of $\mathcal{Z}[\psi]$ over the network ensemble defined by Eq. (2) for finite c , recasting the problem in terms of the solution of a saddle-point integral. More importantly, we give a clear physical interpretation of the order parameters, simplifying the saddle-point equations and obtaining a feasible solution for the dynamics in the sparse regime. In the limit $N \rightarrow \infty$, the microscopic dynamical variables decouple, and the path probability $\mathcal{P}[x]$ for the effective dynamics of a single variable $x(t)$ is determined from

$$\mathcal{P}[x] = \sum_{k=0}^{\infty} p_{\text{in},k} \int \left(\prod_{j=1}^k D x_j \mathcal{P}[x_j] \right) \int \left(\prod_{j=1}^k dJ_j p_J(J_j) \right) \times \delta_F \left[\dot{x}(t) + f[x(t)] - \sum_{j=1}^k J_j g[x(t), x_j(t)] \right], \quad (7)$$

where δ_F is the functional Dirac- δ . The macroscopic observables are computed from $m(t) = \langle x(t) \rangle_*$ and $q(t) = \langle x^2(t) \rangle_*$, where

$$\langle x^n(t) \rangle_* = \int D x x^n(t) \mathcal{P}[x] \quad (n = 1, 2) \quad (8)$$

is the average over the effective dynamics governed by $\mathcal{P}[x]$. The self-consistent Eq. (7) is the exact solution of a broad class of models (see Table I) on sparse directed networks with a local treelike structure [73] and arbitrary distributions p_J and $p_{k,\ell} = p_{\text{in},k} p_{\text{out},\ell}$. In [72], we address the more general case of dynamical models with Gaussian additive noise on networks with correlated indegrees and outdegrees. The solution of Eq. (7) determines the time evolution of the full probability distribution of the microscopic variables in the limit $N \rightarrow \infty$.

Equation (7) is formally similar to other distributional equations appearing in the study of sparse disordered systems [61–66]. Therefore, we can numerically solve this equation using the population dynamics algorithm [61,63,64]. In the standard version of this algorithm [61,64], a probability density is parametrized by a population of stochastic variables. Here, we generalize the algorithm to calculate $\mathcal{P}[x]$ by introducing a population of dynamical trajectories. At each iteration step, a single path is chosen randomly from the population and updated according to the differential equation imposed by the Dirac- δ_F in Eq. (7). After sufficient iterations, the population of paths converges to a stationary distribution, providing a numerical solution for $\mathcal{P}[x]$. A detailed account of the algorithm is in [72].

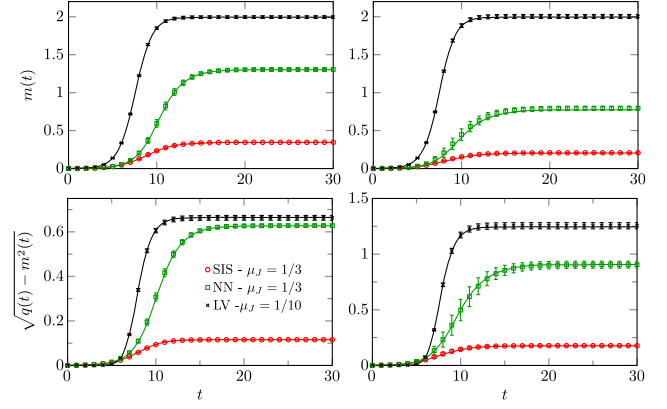


FIG. 1. Dynamics of the mean $m(t)$ and the standard deviation $\sqrt{q(t) - m^2(t)}$ for the SIS model, LV model, and NN model (see Table I). Results are shown for directed random networks with average degree $c = 5$ and two indegree distributions [Eq. (9)]: Poisson (left column) and geometric (right column). The distribution p_J of the coupling strengths has mean μ_J and standard deviation $\sigma_J = 0.1$. For the LV and NN models, p_J is Gaussian; for the SIS model, p_J is uniform. Solid lines are solutions of Eq. (7) using the population dynamics algorithm with 5×10^4 paths and initial condition $x_i(0) = 10^{-3}$. Symbols denote numerical simulations of Eq. (1) for an ensemble of 10 random networks generated from the configuration model with $N = 4000$ nodes. Vertical bars are the standard deviation of the macroscopic observables.

In Fig. 1, we compare the solutions of Eq. (7) with numerical simulations of the original coupled dynamics, Eq. (1), for finite N . The panels showcase the time evolution of the mean $m(t)$ and the standard deviation $\sqrt{q(t) - m^2(t)}$ of the microscopic variables for different network topologies and three models of Table I: the NN model of [1], the LV model, and the SIS model of epidemic spreading. The results in Fig. 1 are for Poisson and geometric indegrees, where $p_{\text{in},k}$ is given by

$$p_{\text{in},k} = \frac{c^k e^{-c}}{k!} \quad \text{and} \quad p_{\text{in},k} = \frac{c^k}{(c+1)^{k+1}}, \quad (9)$$

respectively. In [72], we compare the solutions of Eq. (7) with numerical simulations for two additional cases: the NN model on networks with power-law indegree distributions and the susceptible-infected-susceptible (SIS) model at the epidemic threshold. In all cases, the agreement between our theoretical results for $N \rightarrow \infty$ and numerical simulations for large N is excellent, confirming the exactness of Eq. (7).

An important question is whether Eq. (7) recovers the analytic results of fully connected models as $c \rightarrow \infty$ [1,4,28,30]. By taking the limit $c \rightarrow \infty$ after the thermodynamic limit $N \rightarrow \infty$, we are effectively considering the scaling regime where $c \propto N^a$, with $0 < a < 1$ [74–77]. We show in [72] that, in the limit $c \rightarrow \infty$, degree fluctuations

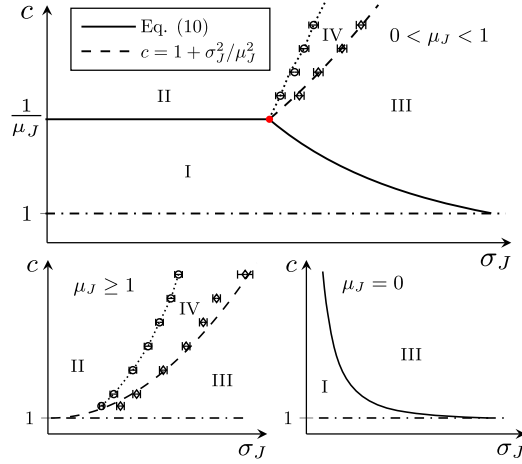


FIG. 2. Phase diagrams (c, σ_J) of the NN model for $\mu_J = 0$, $\mu_J \geq 1$, and $0 < \mu_J < 1$. The average synaptic current $m(t)$ relaxes to trivial and nontrivial fixed points in Phases I and II, respectively. In the chaotic Phases III and IV, $m(t)$ exhibits aperiodic oscillations around zero and nonzero values, respectively (see Fig. 4). The dash-dotted line at $c = 1$ marks the percolation threshold, while the dashed curve identifies the gapless transition. Circles and diamonds represent numerical results for the transition lines delimiting Phase IV (see the main text), obtained from solutions of Eq. (7) using population dynamics with 5×10^4 paths, Poisson indegrees, and two values of μ_J ($\mu_J = 1/3$ and $\mu_J = 3/2$). The red dot marks $(c^*, \sigma_J^*) = [\mu_J^{-1}, \sqrt{\mu_J(1 - \mu_J)}]$.

remain significant, and $\mathcal{P}[x]$ depends on the full distribution $\nu_{\text{in}}(\kappa)$ of rescaled indegrees $\kappa_i = K_i/c$ ($i = 1, \dots, N$). The well-known effective dynamics on fully connected networks is only recovered when $\nu_{\text{in}}(\kappa) = \delta(\kappa - 1)$. This breakdown in the universality of fully connected models due to degree fluctuations was anticipated in [74–77].

Phase diagram of neural networks—To demonstrate the strength of Eq. (7) and its concrete applications, we derive the phase diagram of the NN model on sparse directed networks. In this context, $x_i(t) \in \mathbb{R}$ represents the synaptic current at neuron i , $f(x) = x$, and $g(x, x') = \tanh(x')$. Let us order the complex eigenvalues $\{\lambda_\alpha\}_{\alpha=1, \dots, N}$ of A according to their real parts as $\text{Re}\lambda_1 \geq \text{Re}\lambda_2 \geq \dots \geq \text{Re}\lambda_N$. A linear stability analysis of Eq. (1) shows that $\mathbf{x} = 0$ is stable if $\text{Re}\lambda_1 < 1$. Based on analytic results for the spectra of directed networks for $N \rightarrow \infty$ [67–69], we find that the trivial fixed point is stable provided $c < c_{\text{stab}}$, where

$$c_{\text{stab}} = \begin{cases} 1/\mu_J & \text{if } c > 1 + \sigma_J^2/\mu_J^2, \\ 1/(\sigma_J^2 + \mu_J^2) & \text{if } c \leq 1 + \sigma_J^2/\mu_J^2. \end{cases} \quad (10)$$

The two distinct regimes in Eq. (10) result from the gap-gapless transition in the spectrum of A [67]. For $c > 1 + \sigma_J^2/\mu_J^2$, the spectral gap $|\lambda_1 - \lambda_2|$ remains finite as $N \rightarrow \infty$, while it vanishes for $c \leq 1 + \sigma_J^2/\mu_J^2$. Equation (10) holds for $\mu_J > 0$ and $c > 1$. The condition $c > 1$ ensures

that directed networks with degree distribution $p_{k,\ell} = p_{\text{in},k}p_{\text{out},\ell}$ contain a giant strongly connected component [78,79], implying the existence of a continuous part in the eigenvalue distribution of A [68].

We emphasize that the linear stability analysis of the trivial solution provides no information about the relaxation dynamics or the stationary solutions that emerge when $\mathbf{x} = 0$ becomes unstable. Therefore, we study the dynamics and the stationary states of the NN model by solving Eq. (7). Figure 2 presents the resulting phase diagrams for different regimes of μ_J . In Phase I, $m(t)$ relaxes exponentially fast to the trivial solution $m = 0$, while in Phase II, $m(t)$ evolves to a nonzero fixed point. In Phases III and IV, the neural network exhibits chaotic activity, characterized by slow and aperiodic oscillations of $m(t)$ [1,30]. The stability lines that delimit Phase I are universal, as they depend only on the first and second moments of p_J and $p_{\text{in},k}$.

Figure 3 characterizes the transition between the fixed-point Phases I and II. As c approaches the critical mean degree $c^* = \mu_J^{-1}$ from above, the nontrivial fixed point $m = m(t)$ vanishes continuously. The critical point c^* is independent of $p_{\text{in},k}$ and $m(t)$ relaxes exponentially fast inside Phases I and II. Because of critical slowing down, the numerical solution of Eq. (7) becomes computationally more demanding near c^* . In Phase II, the neuronal firing rates evolve to a stationary distribution with a finite variance. Figure 4 shows the dynamics of $m(t)$ within the chaotic phases for several initial conditions. After a transient time T_{tr} , $m(t)$ stabilizes into an attractor, oscillating around zero in Phase III and around a nonzero value in Phase IV. The inset in Fig. 4(a) demonstrates the sensitivity of $m(t)$ to small perturbations in the initial conditions, characteristic of deterministic chaos [80]. By solving Eq. (7) and numerically computing the temporal averages [81]

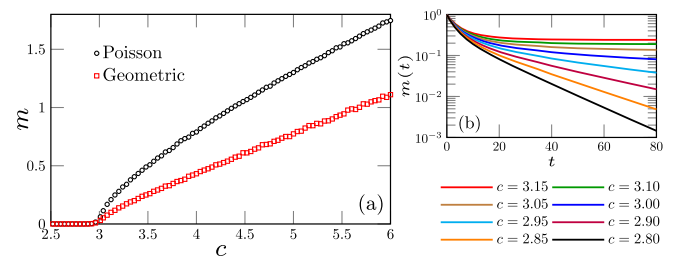


FIG. 3. Continuous transition between the fixed-point phases for the NN model on directed random networks. The coupling strengths follow a Gaussian distribution with mean $\mu_J = 1/3$ and standard deviation $\sigma_J = 0.1$. The results are derived from Eq. (7) using population dynamics with 5×10^4 paths. (a) Fixed-point solution $m(t) = m$ as a function of c for Poisson and geometric indegrees [Eq. (9)]. (b) Relaxation dynamics of $m(t)$ across the transition for Poisson indegrees and initial condition $x_i(0) = 1$. For $c < \mu_J^{-1}$, $m(t)$ relaxes exponentially to $m = 0$ as $t \rightarrow \infty$.

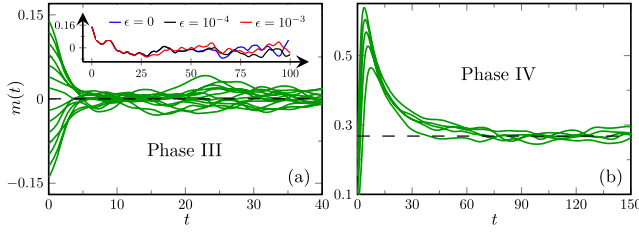


FIG. 4. Dynamics of $m(t)$ inside the chaotic phases for directed networks with Poisson indegrees and a Gaussian distribution p_J with mean $\mu_J = 1/3$. The results follow from the solutions of Eq. (7) using population dynamics with 5×10^4 paths and several initial conditions. The dashed lines indicate the value of M , Eq. (11), characterizing the chaotic attractor in each phase. (a) $c = 2.5$ and $\sigma_J = 2$. Inset: dynamics of $m(t)$ obtained from the deterministic Eq. (1) for a single network instance ($N = 4000$), initial condition $x_i(0) = 0.15 - \epsilon$, and different ϵ . (b) $c = 5$ and $\sigma_J = 0.62$.

$$M = \frac{1}{T - T_{\text{tr}}} \int_{T_{\text{tr}}}^T dt m(t), \quad (11)$$

$$\Delta^2 = \frac{1}{T - T_{\text{tr}}} \int_{T_{\text{tr}}}^T dt [M - m(t)]^2, \quad (12)$$

for $T \gg 1$, we estimate the transition lines delimiting Phase IV [72]. For $T \rightarrow \infty$, the transition between Phases II and IV is determined by Δ , since $\Delta = 0$ in the fixed-point phases and $\Delta > 0$ in the chaotic phases. The parameter M distinguishes the chaotic phases: $M = 0$ in Phase III and $M \neq 0$ in Phase IV (see Fig. 4). Our numerical results for the transition between Phases III and IV are consistent with the dashed line in Fig. 2, suggesting that this transition is governed by the gap $|\lambda_1 - \lambda_2|$ in the network spectrum. Nevertheless, for $c \rightarrow \infty$ this transition to the chaotic Phase III slightly deviates from the gapless transition [30], particularly for large μ_J .

Conclusions—We have developed a dynamical mean-field theory of complex systems on sparse directed networks, deriving an exact path-probability equation for the effective dynamics in the limit $N \rightarrow \infty$. Unlike sparse models with bidirected edges [38,39], our path-probability equation can be numerically solved using population dynamics [64]. We confirmed the exactness of our general solution by comparing it with numerical simulations of fundamental models in the study of epidemic spreading, neural networks, and ecosystems. Finally, we applied our solution to determine the complete phase diagram of the sparse and directed version of the canonical neural network model of [1,30].

The numerical solution of Eq. (7) does not require generating networks from the configuration model [71], providing moderate computational advantages over large-scale simulations of Eq. (1) on networks [22]. Beyond its numerical applications, Eq. (7) provides a foundational framework for studying the stationary states [4], computing

correlation functions [3], deriving approximate dynamical equations for macroscopic order parameters, and developing systematic perturbative approaches [26,82].

Our work paves the way for exploring the role of sparse heterogeneous networks on the dynamics of ecosystems, coupled oscillators, epidemic spreading, and beyond. Future works include determining the phase diagram of the sparse Lotka-Volterra model [7], the influence of external noise on phase diagrams [29], and the role of network heterogeneities on the critical exponents of complex systems [77,83]. Lastly, it would be interesting to connect the present formalism with the cavity method in [84].

Acknowledgments—F.L.M. thanks Tuan Minh Pham and Alessandro Ingrosso for many stimulating discussions. The author also thanks Thomas Peron and Tuan Minh Pham for their valuable comments on the manuscript. F.L.M. acknowledges support from CNPq (Grant No 402487/2023-0) and from the ICTP through the Associates Program (2023-2028).

-
- [1] H. Sompolsky, A. Crisanti, and H. J. Sommers, Chaos in random neural networks, *Phys. Rev. Lett.* **61**, 259 (1988).
 - [2] Jonathan Kadmon and Haim Sompolsky, Transition to chaos in random neuronal networks, *Phys. Rev. X* **5**, 041030 (2015).
 - [3] Daniel Martí, Nicolas Brunel, and Srdjan Ostojic, Correlations between synapses in pairs of neurons slow down dynamics in randomly connected neural networks, *Phys. Rev. E* **97**, 062314 (2018).
 - [4] A. Crisanti and H. Sompolsky, Path integral approach to random neural networks, *Phys. Rev. E* **98**, 062120 (2018).
 - [5] Carles Martorell, Rubén Calvo, Alessia Annibale, and Miguel A. Muñoz, Dynamically selected steady states and criticality in non-reciprocal networks, *Chaos, Solitons Fractals* **182**, 114809 (2024).
 - [6] Manfred Opper and Sigurd Diederich, Phase transition and 1/f noise in a game dynamical model, *Phys. Rev. Lett.* **69**, 1616 (1992).
 - [7] Guy Bunin, Ecological communities with Lotka-Volterra dynamics, *Phys. Rev. E* **95**, 042414 (2017).
 - [8] Ada Altieri, Felix Roy, Chiara Cammarota, and Giulio Biroli, Properties of equilibria and glassy phases of the random Lotka-Volterra model with demographic noise, *Phys. Rev. Lett.* **126**, 258301 (2021).
 - [9] Angélica S. Mata and Silvio C. Ferreira, Pair quenched mean-field theory for the susceptible-infected-susceptible model on complex networks, *Europhys. Lett.* **103**, 48003 (2013).
 - [10] P. Van Mieghem, Epidemic phase transition of the SIS type in networks, *Europhys. Lett.* **97**, 48004 (2012).
 - [11] A. V. Goltsev, S. N. Dorogovtsev, J. G. Oliveira, and J. F. F. Mendes, Localization and spreading of diseases in complex networks, *Phys. Rev. Lett.* **109**, 128702 (2012).

- [12] Romualdo Pastor-Satorras, Claudio Castellano, Piet Van Mieghem, and Alessandro Vespignani, Epidemic processes in complex networks, *Rev. Mod. Phys.* **87**, 925 (2015).
- [13] J. C. Stiller and G. Radons, Dynamics of nonlinear oscillators with random interactions, *Phys. Rev. E* **58**, 1789 (1998).
- [14] Francisco A. Rodrigues, Thomas K. DM. Peron, Peng Ji, and Jürgen Kurths, The Kuramoto model in complex networks, *Phys. Rep.* **610**, 1 (2016).
- [15] Axel Prüser, Sebastian Rosmej, and Andreas Engel, Nature of the volcano transition in the fully disordered Kuramoto model, *Phys. Rev. Lett.* **132**, 187201 (2024).
- [16] Fabian Baumann, Philipp Lorenz-Spreen, Igor M. Sokolov, and Michele Starnini, Modeling echo chambers and polarization dynamics in social networks, *Phys. Rev. Lett.* **124**, 048301 (2020).
- [17] Fabian Baumann, Philipp Lorenz-Spreen, Igor M. Sokolov, and Michele Starnini, Emergence of polarized ideological opinions in multidimensional topic spaces, *Phys. Rev. X* **11**, 011012 (2021).
- [18] Claude Godrèche and Jean-Marc Luck, Characterising the nonequilibrium stationary states of Ornstein–Uhlenbeck processes, *J. Phys. A* **52**, 035002 (2018).
- [19] Andrea Crisanti and Matteo Paoluzzi, Most probable path of active Ornstein-Uhlenbeck particles, *Phys. Rev. E* **107**, 034110 (2023).
- [20] Francesco Ferraro, Christian Grilletta, Amos Maritan, Samir Suweis, and Sandro Azaele, Exact solution of dynamical mean-field theory for a linear system with annealed disorder, [arXiv:2405.05183](https://arxiv.org/abs/2405.05183).
- [21] I. Z. Kiss, J. C. Miller, and P. L. Simon, *Mathematics of Epidemics on Networks: From Exact to Approximate Models*, Interdisciplinary Applied Mathematics (Springer International Publishing, New York, 2017).
- [22] Diogo H. Silva, Francisco A. Rodrigues, and Silvio C. Ferreira, High prevalence regimes in the pair-quenched mean-field theory for the susceptible-infected-susceptible model on networks, *Phys. Rev. E* **102**, 012313 (2020).
- [23] V. Thibault, A. Allard, and P. Desrosiers, The low-rank hypothesis of complex systems, *Nat. Phys.* **20**, 294 (2024).
- [24] P. C. Martin, E. D. Siggia, and H. A. Rose, Statistical dynamics of classical systems, *Phys. Rev. A* **8**, 423 (1973).
- [25] A. C. C. Coolen, Chapter 15 statistical mechanics of recurrent neural networks II—dynamics, in *Neuro-Informatics and Neural Modelling*, Handbook of Biological Physics Vol. 4, edited by F. Moss and S. Gielen (North-Holland, Amsterdam, 2001), pp. 619–684.
- [26] John A Hertz, Yasser Roudi, and Peter Sollich, Path integral methods for the dynamics of stochastic and disordered systems, *J. Phys. A* **50**, 033001 (2016).
- [27] F Roy, G Biroli, G Bunin, and C Cammarota, Numerical implementation of dynamical mean field theory for disordered systems: Application to the Lotka–Volterra model of ecosystems, *J. Phys. A* **52**, 484001 (2019).
- [28] Tobias Galla, Dynamically evolved community size and stability of random Lotka-Volterra ecosystems(a), *Europhys. Lett.* **123**, 48004 (2018).
- [29] Jannis Schuecker, Sven Goedeke, and Moritz Helias, Optimal sequence memory in driven random networks, *Phys. Rev. X* **8**, 041029 (2018).
- [30] Francesca Mastrogiuseppe and Srdjan Ostojic, Linking connectivity, dynamics, and computations in low-rank recurrent neural networks, *Neuron* **99**, 609 (2018).
- [31] Lyle Poley, Joseph W. Baron, and Tobias Galla, Generalized Lotka-Volterra model with hierarchical interactions, *Phys. Rev. E* **107**, 024313 (2023).
- [32] Fabián Aguirre-López, Heterogeneous mean-field analysis of the generalized Lotka-Volterra model on a network, *J. Phys. A* **57**, 345002 (2024).
- [33] Jong Il Park, Deok-Sun Lee, Sang Hoon Lee, and Hye Jin Park, Incorporating heterogeneous interactions for ecological biodiversity, *Phys. Rev. Lett.* **133**, 198402 (2024).
- [34] Tuan Minh Pham and Kuniyiko Kaneko, Dynamical theory for adaptive systems, *J. Stat. Mech.* **113501** (2024).
- [35] Valentina Ros, Felix Roy, Giulio Biroli, and Guy Bunin, Quenched complexity of equilibria for asymmetric generalized Lotka–Volterra equations, *J. Phys. A* **56**, 305003 (2023).
- [36] M. Newman, *Networks: An Introduction* (Oxford University Press, Oxford, 2010).
- [37] Paulo R. Guimarães, The structure of ecological networks across levels of organization, *Annu. Rev. Ecol. Evol. Syst.* **51**, 433 (2020).
- [38] J. P. L. Hatchett, B. Wemmenhove, I. Pérez Castillo, T. Nikolettopoulos, N. S. Skantzios, and A. C. C. Coolen, Parallel dynamics of disordered Ising spin systems on finitely connected random graphs, *J. Phys. A* **37**, 6201 (2004).
- [39] I. Neri and D. Bollé, The cavity approach to parallel dynamics of Ising spins on a graph, *J. Stat. Mech.* (2009) P08009.
- [40] Kazushi Mimura and A. C. C. Coolen, Parallel dynamics of disordered Ising spin systems on finitely connected directed random graphs with arbitrary degree distributions, *J. Phys. A* **42**, 415001 (2009).
- [41] Yasser Roudi and John Hertz, Dynamical tap equations for non-equilibrium Ising spin glasses, *J. Stat. Mech.* (2011) P03031.
- [42] Erik Aurell and Hamed Mahmoudi, Dynamic mean-field and cavity methods for diluted Ising systems, *Phys. Rev. E* **85**, 031119 (2012).
- [43] P. Zhang, Inference of kinetic Ising model on sparse graphs, *J. Stat. Phys.* **148**, 502 (2012).
- [44] Gino Del Ferraro and Erik Aurell, Dynamic message-passing approach for kinetic spin models with reversible dynamics, *Phys. Rev. E* **92**, 010102(R) (2015).
- [45] E. Aurell, G. Del Ferraro, E. Domínguez, and R. Mulet, Cavity master equation for the continuous time dynamics of discrete-spin models, *Phys. Rev. E* **95**, 052119 (2017).
- [46] Eduardo Domínguez Vázquez, Gino Del Ferraro, and Federico Ricci-Tersenghi, A simple analytical description of the non-stationary dynamics in Ising spin systems, *J. Stat. Mech.* (2017) 033303.
- [47] Giuseppe Torrisi, Alessia Annibale, and Reimer Kühn, Overcoming the complexity barrier of the dynamic message-passing method in networks with fat-tailed degree distributions, *Phys. Rev. E* **104**, 045313 (2021).
- [48] Giuseppe Torrisi, Reimer Kühn, and Alessia Annibale, Uncovering the non-equilibrium stationary properties in sparse boolean networks, *J. Stat. Mech.* (2022) 053303.

- [49] Freya Behrens, Barbora Hudcová, and Lenka Zdeborová, Backtracking dynamical cavity method, *Phys. Rev. X* **13**, 031021 (2023).
- [50] Freya Behrens, Barbora Hudcová, and Lenka Zdeborová, Dynamical phase transitions in graph cellular automata, *Phys. Rev. E* **109**, 044312 (2024).
- [51] B. Derrida, E. Gardner, and A. Zippelius, An exactly solvable asymmetric neural network model, *Europhys. Lett.* **4**, 167 (1987).
- [52] Malbor Asllani, Renaud Lambiotte, and Timoteo Carletti, Structure and dynamical behavior of non-normal networks, *Sci. Adv.* **4**, eaau9403 (2018).
- [53] Yangfan Peng, Antje Bjelde, Pau Vilimelis Aceituno, Franz X. Mittermaier, Henrike Planert, Sabine Grosser, Julia Onken, Katharina Faust, Thilo Kalbhenn, Matthias Simon, Helena Radbruch, Pawel Fidzinski, Dietmar Schmitz, Henrik Alle, Martin Holtkamp, Imre Vida, Benjamin F. Grewe, and Jörg R. P. Geiger, Directed and acyclic synaptic connectivity in the human layer 2-3 cortical microcircuit, *Science* **384**, 338 (2024).
- [54] Jennifer A. Dunne, Richard J. Williams, and Neo D. Martinez, Food-web structure and network theory: The role of connectance and size, *Proc. Natl. Acad. Sci. U.S.A.* **99**, 12917 (2002).
- [55] Jordi Bascompte, Disentangling the web of life, *Science* **325**, 416 (2009).
- [56] S. S. Shen-Orr, R. Milo, S. Mangan, and U. Alon, Network motifs in the transcriptional regulation network of *Escherichia coli*, *Nat. Genet.* **31**, 64 (2002).
- [57] Tong Ihn Lee *et al.*, Transcriptional regulatory networks in *Saccharomyces cerevisiae*, *Science* **298**, 799 (2002).
- [58] Haewoon Kwak, Changhyun Lee, Hosung Park, and Sue Moon, What is twitter, a social network or a news media? in *Proceedings of the 19th International Conference on World Wide Web* (Association for Computing Machinery, New York, USA, 2010), pp. 591–600.
- [59] Christoph Schweimer, Christine Gfrerer, Florian Lugstein, David Pape, Jan A. Velimsky, Robert Elsässer, and Bernhard C. Geiger, *Generating Simple Directed Social Network Graphs for Information Spreading* (Association for Computing Machinery, New York, USA, 2022), pp. 1475–1485.
- [60] R. Pastor-Satorras and A. Vespignani, *Evolution and Structure of the Internet: A Statistical Physics Approach* (Cambridge University Press, Cambridge, England, 2004).
- [61] M. Mézard and G. Parisi, The Bethe lattice spin glass revisited, *Eur. Phys. J. B* **20**, 217 (2001).
- [62] M. Mézard and G. Parisi, The cavity method at zero temperature, *J. Stat. Phys.* **111**, 1 (2003).
- [63] Reimer Kühn, Spectra of sparse random matrices, *J. Phys. A* **41**, 295002 (2008).
- [64] Fernando Lucas Metz, Izaak Neri, and Tim Rogers, Spectral theory of sparse non-Hermitian random matrices, *J. Phys. A* **52**, 434003 (2019).
- [65] R. Abou-Chacra, D. J. Thouless, and P. W. Anderson, A self-consistent theory of localization, *J. Phys. C* **6**, 1734 (1973).
- [66] M. Mézard and A. Montanari, *Information, Physics, and Computation*, Oxford Graduate Texts (Oxford University Press, Oxford, 2009).
- [67] Izaak Neri and Fernando Lucas Metz, Eigenvalue outliers of non-Hermitian random matrices with a local tree structure, *Phys. Rev. Lett.* **117**, 224101 (2016).
- [68] Izaak Neri and Fernando Lucas Metz, Linear stability analysis of large dynamical systems on random directed graphs, *Phys. Rev. Res.* **2**, 033313 (2020).
- [69] Fernando Lucas Metz and Izaak Neri, Localization and universality of eigenvectors in directed random graphs, *Phys. Rev. Lett.* **126**, 040604 (2021).
- [70] M. E. J. Newman, S. H. Strogatz, and D. J. Watts, Random graphs with arbitrary degree distributions and their applications, *Phys. Rev. E* **64**, 026118 (2001).
- [71] Bailey K. Fosdick, Daniel B. Larremore, Joel Nishimura, and Johan Ugander, Configuring random graph models with fixed degree sequences, *SIAM Rev.* **60**, 315 (2018).
- [72] See Supplemental Material at <http://link.aps.org/supplemental/10.1103/PhysRevLett.134.037401> for all derivations of DMFT and a detailed account of the population dynamics algorithm.
- [73] Charles Bordenave and Marc Lelarge, Resolvent of large random graphs, *Random Struct. Algorithms* **37**, 332 (2010).
- [74] Fernando L. Metz and Jeferson D. Silva, Spectral density of dense random networks and the breakdown of the Wigner semicircle law, *Phys. Rev. Res.* **2**, 043116 (2020).
- [75] Fernando L. Metz and Thomas Peron, Mean-field theory of vector spin models on networks with arbitrary degree distributions, *J. Phys.: Complexity* **3**, 015008 (2022).
- [76] Jeferson D. Silva and Fernando L. Metz, Analytic solution of the resolvent equations for heterogeneous random graphs: Spectral and localization properties, *J. Phys.: Complexity* **3**, 045012 (2022).
- [77] Leonardo S. Ferreira and Fernando L. Metz, Nonequilibrium dynamics of the Ising model on heterogeneous networks with an arbitrary distribution of threshold noise, *Phys. Rev. E* **107**, 034127 (2023).
- [78] G. Timár, A. V. Goltsev, S. N. Dorogovtsev, and J. F. F. Mendes, Mapping the structure of directed networks: Beyond the bow-tie diagram, *Phys. Rev. Lett.* **118**, 078301 (2017).
- [79] Ivan Kryven, Emergence of the giant weak component in directed random graphs with arbitrary degree distributions, *Phys. Rev. E* **94**, 012315 (2016).
- [80] G. L. Baker and J. P. Gollub, *Chaotic Dynamics: An Introduction* (Cambridge University Press, Cambridge, England, 1996).
- [81] Maximilian Gelbrecht, Jürgen Kurths, and Frank Hellmann, Monte Carlo basin bifurcation analysis, *New J. Phys.* **22**, 033032 (2020).
- [82] F. L. Metz, G. Parisi, and L. Leuzzi, Finite-size corrections to the spectrum of regular random graphs: An analytical solution, *Phys. Rev. E* **90**, 052109 (2014).
- [83] Thibaut Arnoux de Pirey and Guy Bunin, Critical behavior of a phase transition in the dynamics of interacting populations, [arXiv:2402.05063](https://arxiv.org/abs/2402.05063).
- [84] Mattia Tarabolo and Luca Dall'Asta, Gaussian approximation of dynamic cavity equations for linearly-coupled stochastic dynamics, [arXiv:2406.14200](https://arxiv.org/abs/2406.14200).